JACS
JOURNAL OF THE AMERICAN CHEMICAL SOCIETY

Article

pubs.acs.org/JACS

Discriminative Separation of Gases by a "Molecular Trapdoor" Mechanism in Chabazite Zeolites

Jin Shang,[†,‡,◆] Gang Li,[†,‡,◆] Ranjeet Singh,[†,‡] Qinfen Gu,[§] Kate M. Nairn,[∥,#] Timothy J. Bastow,[▽] Nikhil Medhekar,[∥] Cara M. Doherty,[▽] Anita J. Hill,[▽,○] Jefferson Z. Liu,*[,⊥] and Paul A. Webley*[,†,‡]

[†]Cooperative Research Centre for Greenhouse Gas Technologies (CO2CRC), Melbourne, Australia

[‡]Department of Chemical and Biomolecular Engineering, The University of Melbourne, Melbourne, Victoria 3010, Australia

[§]Australian Synchrotron, 800 Blackburn Rd, Clayton, Victoria 3168, Australia

[∥]Department of Materials Engineering and [⊥]Department of Mechanical and Aerospace Engineering, Monash University, Clayton, Victoria 3800, Australia

[#]ARC Centre of Excellence for Electromaterials Science, Clayton, Victoria, Australia

[▽]CSIRO Materials Science and Engineering, Clayton, Victoria 3169, Australia

[○]CSIRO Process Science and Engineering, Clayton, Victoria 3169, Australia

Supporting Information

ABSTRACT: Separation of molecules based on molecular size in zeolites with appropriate pore aperture dimensions has given rise to the definition of "molecular sieves" and has been the basis for a variety of separation applications. We show here that for a class of chabazite zeolites, what appears to be "molecular sieving" based on dimension is actually separation based on a difference in ability of a guest molecule to induce temporary and reversible cation deviation from the center of pore apertures, allowing for exclusive admission of certain molecules. This new mechanism of discrimination permits "size-inverse" separation: we illustrate the case of admission of a larger molecule (CO) in preference to a smaller molecule (N_2). Through a combination of experimental and computational approaches, we have uncovered the underlying mechanism and show that it is similar to a "molecular trapdoor". Our materials show the highest selectivity of CO_2 over CH_4 reported to date with important application to natural gas purification.

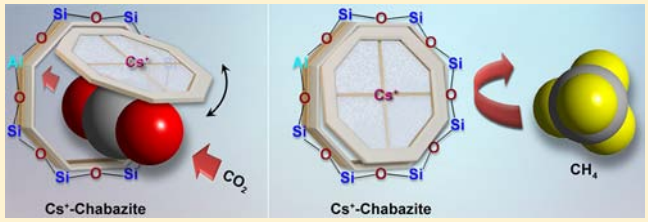

INTRODUCTION

Zeolite molecular sieves are one of the most important materials for separation of molecules. Molecular sieving is conventionally defined as separation based on the differences in size and/or shape between the pore aperture and guest molecules,[1] and this underlying premise has prevailed for many decades. Separation by sieving can, in principle, provide an infinitely high selectivity for molecules of different sizes or shapes, such as CO_2/N_2 separation on ETS-4[2] and xylene isomer separation on MFI.[3] If molecular sieving was based purely on size, however, it would not allow for selective uptake of the larger component in a gas mixture, e.g., CO (kinetic diameter σ = 3.76 Å) over N_2 (σ = 3.64 Å). To achieve such a separation would require a different mechanism. Here, we report a "molecular trapdoor" mechanism in specifically tailored chabazite (CHA) zeolites that produces a counterintuitive size-inverse "sieving" for CO/N_2 and a record high selectivity for CO_2/CH_4 separation over a large pressure range.

Chabazite[4] (Figures 1a and S1, Supporting Information), a typical small-pore zeolite, has a three-dimensional structure that consists of double six-ring prisms (D6Rs) arranged in layers linked by tilted four-membered rings (4MRs). Although large supercavities (6.7 × 10 Å) exist in the structure, eight-membered rings (8MRs) (Figure 1B) that are 3.8 × 3.8 Å in diameter function as apertures or "doorways", providing access to the crystal interior. A key feature of chabazite is that the extraframework cations required to balance the framework charge may coordinate in the 8MRs (at site SIII′) and thus affect the accessibility of the supercavities. This is commonly observed for a large group of small-pore zeolites with similar 8MRs in their framework, such as LTA[5] and RHO.[6]

RESULTS AND DISCUSSION

Temperature-Dependent Gas Admission in Chabazite. We have synthesized a series of chabazite materials with various silicon-to-aluminum ratios (Si:Al) and cation types and performed adsorption experiments with CO_2, N_2, and CH_4. We observed that the accessibility of adsorption sites (within the supercavities) of certain types of chabazite to gas molecules is nonmonotonically temperature dependent, such that a particular type of gas can only be adsorbed above a certain

Received: September 19, 2012
Published: October 30, 2012

   dx.doi.org/10.1021/ja309274y | J. Am. Chem. Soc. 2012, 134, 19246−19253

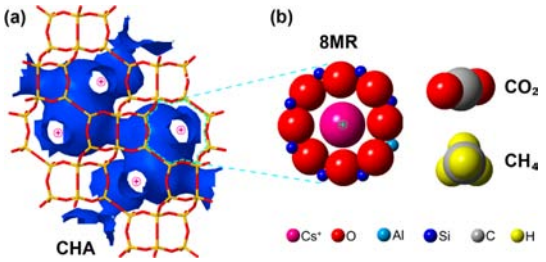

Figure 1. Schematic illustration of the chabazite–gas system. (a) The framework of chabazite (CHA) with eight-membered rings (8MRs) (3.8 × 3.8 Å) as the only access to the crystal interior. The channel surface is illustrated in blue. (b) Representation of one 8MR (doorway) with a "door-keeping" cesium cation (diameter 3.34 Å) at the center of the 8MR (site SIII′) and comparison with relevant gas molecules CO_2 (kinetic diameter σ = 3.3 Å) and CH_4 (σ = 3.8 Å). The open/cation-free pore aperture size is defined by subtracting twice the oxygen radius (1.35 Å) from the distance between the centers of the farthest opposite oxygen atoms. The pore aperture with blocking cation available for gas diffusion is much smaller than the size of all the gases studied in our experiments. The sizes of all atoms and bonds are shown in proportion.

temperature, which we denote as the critical admission temperature (T_C) or the so-called pore-blockage[7] temperature for that specific gas. As shown in Figure 2a, a potassium chabazite with Si:Al = 2.2 (denoted **r2**KCHA) exhibited negligible CH_4 and N_2 adsorption (N_2 surface area of only 20 m^2/g, as shown in Table S2, Supporting Information) below 279 and 266 K, respectively, but noticeable uptake at higher temperatures.[8] Similar behavior on cesium chabazite with Si:Al = 2.5 (**r2**CsCHA) was also observed (Figure 2b), with $T_C(N_2)$ = 333 K and $T_C(CH_4)$ = 343 K. However, T_C is absent for CO_2 on the above two chabazites, indicating no pore-blockage for CO_2 adsorption even at temperatures down to 195 K. Decreasing Si:Al to 1.2 in potassium chabazite (**r1**KCHA), we observed an increase of $T_C(N_2)$ (Figure 2c) as compared with that on **r2**KCHA.

The existence of a critical admission temperature provides us with an opportunity to achieve selective admission of gases. Indeed, at temperatures below 253 K for **r2**CsCHA and 273 K for **r1**KCHA, the materials exhibit exceptionally high selectivities of CO_2 over N_2 and CH_4, respectively, over a large pressure range (Figure 2d,e). At 100 kPa, **r1**KCHA shows pure component selectivities[9] of CO_2/CH_4 and CO_2/N_2 of 93 and 80, respectively. These are suggestive of a separation efficiency that can only be reached by molecular sieving, within the regime of physisorption.

A similar temperature-dependent behavior has been observed before in the context of gas encapsulation in LTA zeolite.[1] It

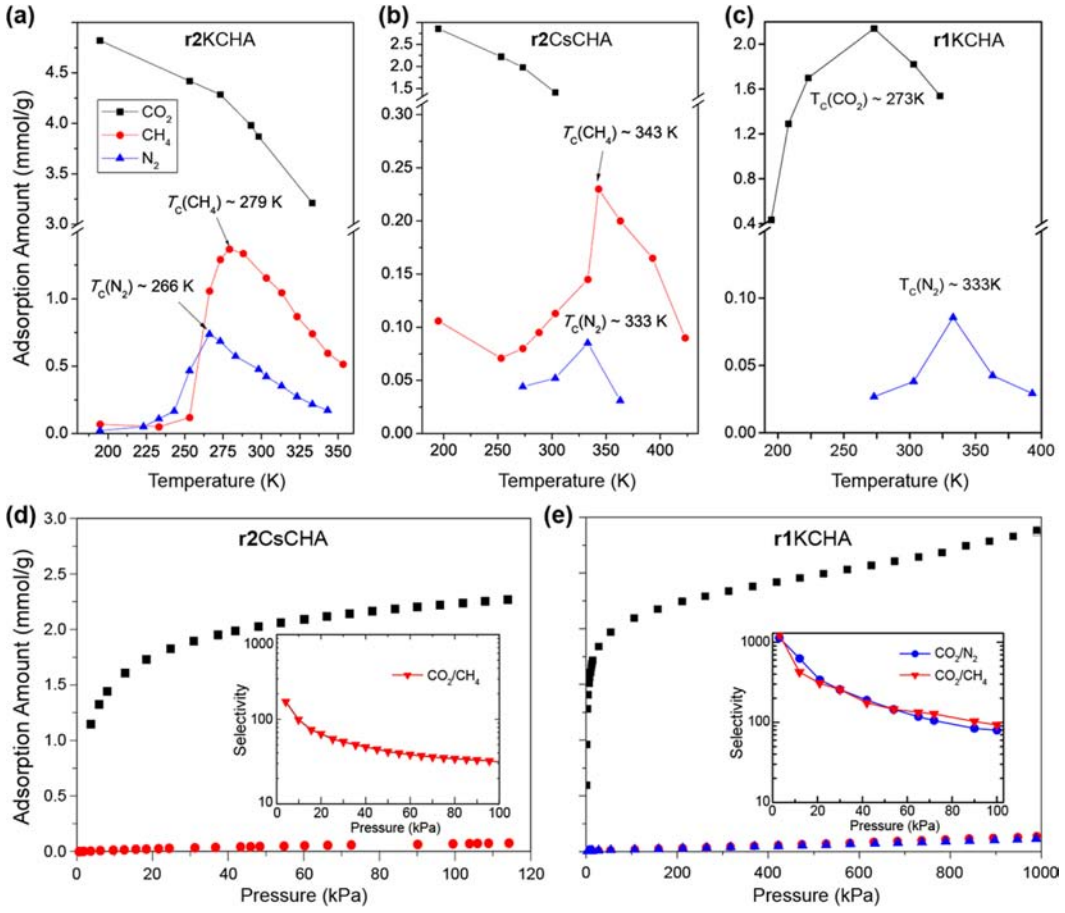

Figure 2. (a, b) Isobars of CO_2, N_2, and CH_4 at 100 kPa showing the existence of critical "pore-blockage" temperatures (T_C) for N_2 and CH_4 and the absence of T_C for CO_2 over the temperature range studied on (a) **r2**KCHA and (b) **r2**CsCHA. For the same gas, T_C is higher on **r2**CsCHA. (c) Isobars of CO_2 and N_2 at 100 kPa on **r1**KCHA demonstrating the existence of T_C for both gases. (d) Adsorption isotherms of CO_2 and CH_4 at 253 K and CO_2/CH_4 selectivities (inset) on **r2**CsCHA. (e) Adsorption isotherms of CO_2, N_2, and CH_4 at 273 K up to 10 bar of pressure and CO_2/N_2 and CO_2/CH_4 selectivities (inset) on **r1**KCHA. Lines are guides to the eye.

dx.doi.org/10.1021/ja309274y | J. Am. Chem. Soc. 2012, 134, 19246–19253

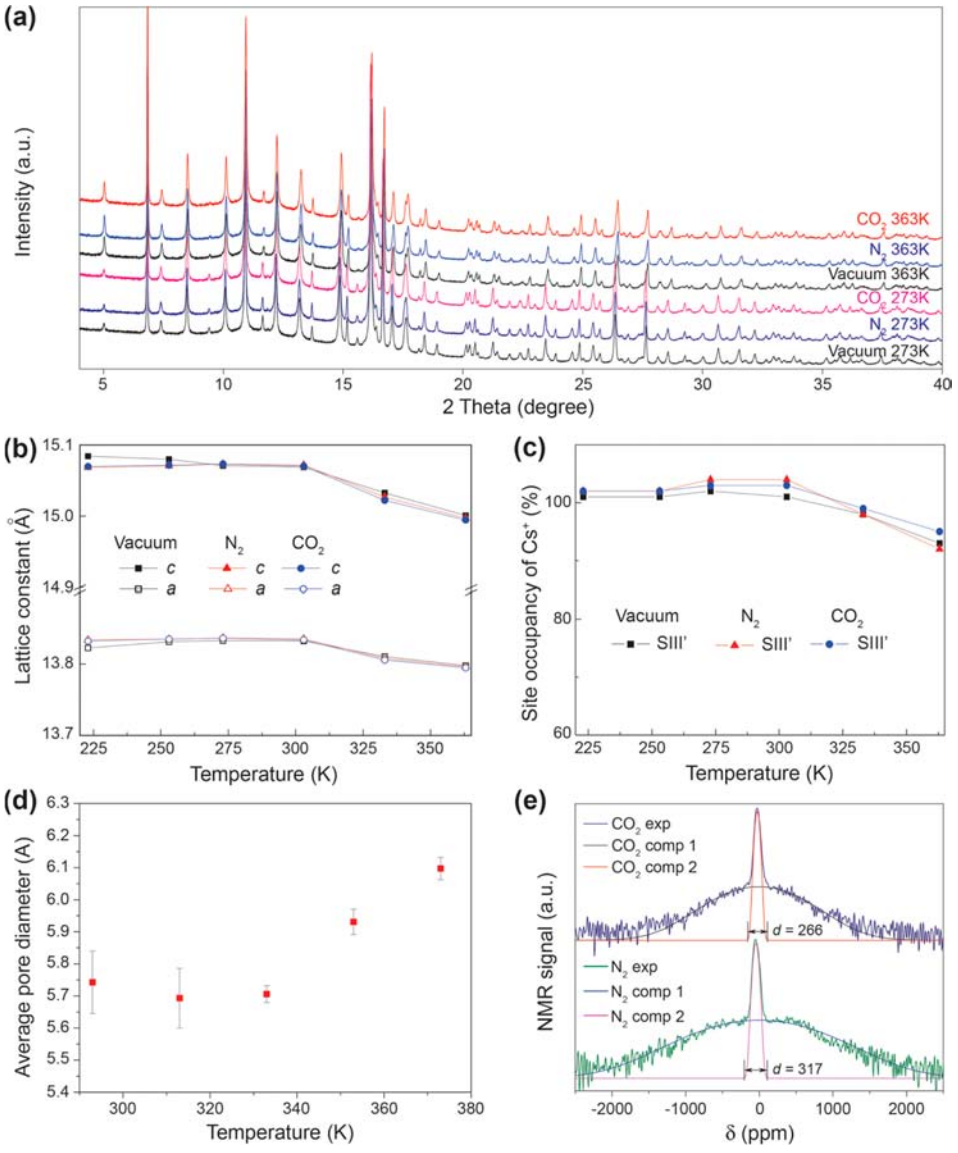

Figure 3. (a) Synchrotron PXRD patterns of **r2**CsCHA at indicated conditions. (b) Lattice parameters and (c) site SIII′ occupancy (doorway) of Cs^+ as a function of temperature under various atmospheres determined by synchrotron PXRD. The estimated error in lattice constant is 0.3% and the error of site occupancy is 1.5%. No thermal expansion is observed over the whole temperature range studied. Above 303−333 K, SIII′ site occupancy reduced from 100%, leading to the opening of pore apertures. (d) Average pore diameter as a function of temperature determined by PALS. An abrupt change is observed above 330 K, which correlates well with the reduction of SIII′ site occupancy shown in c. (e) The mobility of Cs^+ at 295 K in the presence of N_2 and CO_2, respectively (gases loaded at high temperature >363 K), determined by ^{133}Cs NMR on **r2**CsCHA, indicating a higher mobility of Cs^+ in the CO_2 atmosphere. The vertical coordinate is on a logarithm scale with arbitrary units. Fitting results: N_2 component 1 (69% of area, ∼0 ppm, 2000 ppm fwhm), N_2 component 2 (31% of area, −47 ppm, 89 ppm fwhm), CO_2 component 1 (63% of area, ∼0 ppm, 1434 ppm fwhm), and CO_2 component 2 (37% of area, −28 ppm, 79 ppm fwhm). Lines are guides to the eye.

has been attributed variously to the thermal dilation of the pore apertures, "pulsation" of the aperture atoms, and the activated diffusion of the gas molecules at elevated temperatures.[1,10] However, these explanations are not applicable to our case, as evidenced by our experimental measurements. Synchrotron powder X-ray diffraction (PXRD) measurements for **r2**CsCHA (Figure 3a,b) in various gas environments (CO_2, N_2, and vacuum) and over a range of temperatures clearly show that the lattice parameters *a* and *c* remain almost unchanged below 303−333 K and then decrease above 333 K, indicating a negative thermal expansion.[11] Resolving the PXRD signals (e.g., Tables S3 and S4 and Figure S2, Supporting Information) reveals that the Cs cations are positioned in the very center of the 8MRs (site SIII′) and the occupancy of site SIII′ is 100% below 303−333 K (Figure 2C). Considering that the diameter of Cs^+ is 3.34 Å and that of the cation-free 8MR aperture is about 3.8 Å, we can also rule out the explanations of the pulsation of the aperture atoms and the activated diffusion of gas molecules such as CO_2 (σ = 3.3 Å), N_2 (σ = 3.64 Å), and CH_4 (σ = 3.8 Å) through the completely cation-blocked 8MRs, given that all of the 8MR doorways are closed below 303−333 K.[12] Therefore, admission of any molecule into the supercavity is only possible if the door-keeping cation (at site SIII′) migrates at least partially away from the 8MR, under internal or external stimuli.

Gas Admission by Thermally Induced Cation Migration. As shown by synchrotron PXRD (Figure 3c), the occupancy of site SIII′ by Cs^+ dropped to about 90−95% when

dx.doi.org/10.1021/ja309274y | J. Am. Chem. Soc. 2012, 134, 19246−19253

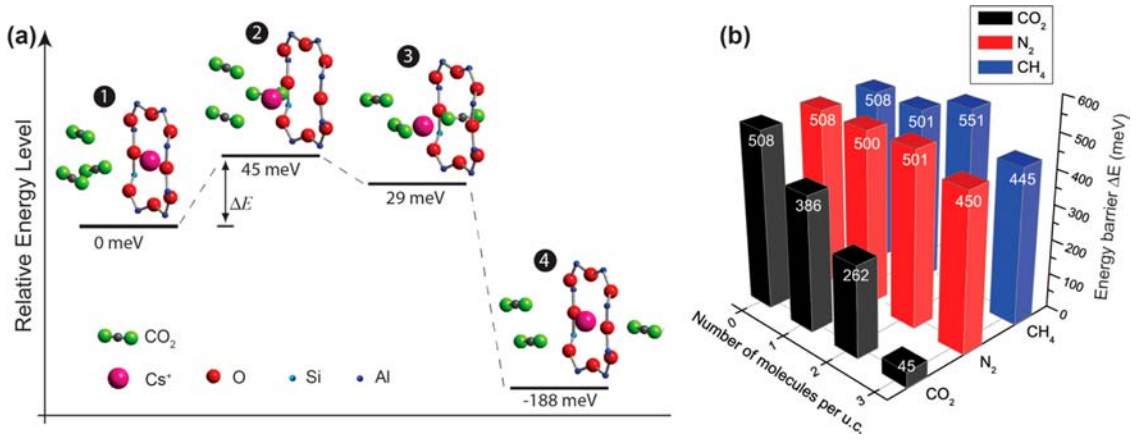

Figure 4. (a) Illustration of the molecular trapdoor mechanism and the corresponding energy levels calculated by DFT for the case in which three CO_2 molecules are initially present in the "guest-rich" side (left-hand side) of the 8MR. State 1, closed state of trapdoor on exposure to CO_2 gas molecules. State 2, guest molecules induce Cs^+ deviation away from the center of the 8MR doorway, resembling the opening of the trapdoor. This state corresponds to the highest energy level of the system. State 3, one CO_2 molecule moves into the doorway and binds to the 8MR. State 4, the CO_2 molecule passes through the doorway and moves further into the guest-lean side (another supercavity) of the 8MR. Sequentially, the Cs^+ returns to its initial position spontaneously, reaching the energy minimum of the system. (b) Comparison of energy barriers ΔE for cation deviation away from 8MR centers (from state 1 to state 2 in part a) in **r2**CsCHA by DFT calculations. The presence of CO_2 molecules substantially reduces the ΔE in contrast to N_2 and CH_4.

the system temperature rose above 303−333 K, indicating the spontaneous migration of a fraction of Cs^+ away from the 8MRs. This migration leads to complete opening of a fraction of 8MR doorways and allows for admission of gas molecules into the chabazite supercavities. This trend is the same for vacuum and gases (CO_2 and N_2), suggesting these gas molecules have little effect on the spontaneous migration of door-keeping cations. Such a spontaneous cation migration is an intrinsic property of the material occurring above a threshold temperature denoted here as T_S (303−333 K for **r2**CsCHA). The spontaneous cation migration above T_S is also supported by our positron annihilation lifetime spectroscopy (PALS) experiments under vacuum (Figure 3d). For **r2**CsCHA, the average pore size measured by PALS displays an abrupt increase above 330 K. Since the average pore size is interpreted to be proportional to the accessible volume in a three-dimensional network,[11] this increase of PALS-interpreted average pore size (Figure 3d) corresponds to the available interconnection between neighboring supercavities via cation-free 8MRs. We note that T_S correlates very well to the observed critical admission temperatures T_C for N_2 (~333 K) and CH_4 (~343 K), as shown in the experimental adsorption isobars (Figure 2b). On the basis of the above experimental evidence, we conclude that spontaneous thermal migration of door-keeping cations is responsible for the admission of N_2 and CH_4 above T_S.

Admission by Guest-Induced Cation Deviation—Molecular Trapdoor Mechanism. The question still remains: How does CO_2 access the supercavities through the cation-blocked 8MR even below T_S? It appears that substantial adsorption of CO_2 occurred (Figure 2b) while all the "doors" were closed below 303−330 K. We hypothesize that CO_2 must have entered the supercavities through the 8MR doorway by inducing deviation of the door-keeping Cs^+ (i.e., partially moving away from centers of the 8MRs without reaching other stable cation sites) temporarily and reversibly. This is distinct from the permanent thermally induced cation migration discussed in the previous section.

For cations such as Cs^+ [13] and K^+,[14] the SIII′ sites in the center of the 8MRs of chabazite are the energetically favorable positions, hence the term door-keeping cations, which is consistent with our density functional theory (DFT) calculations (Table S1, Figure S3, Supporting Information). Successful passage of gas molecules through such cation-blocked 8MRs occurs only when the cations deviate away from the center of 8MRs. This can be accomplished by either increasing the thermal kinetic energy of the cations or changing the potential well experienced by the door-keeping cations (Figure S3, Supporting Information) under the influence of the guest molecules. Guest molecules, such as CO_2, can strongly interact with the cation and substantially lower the potential well of door-keeping cations in the gas molecule side of the 8MRs (which can be quantitatively represented by the reduction of the energy barrier ΔE). The thermal vibration of the cations causes their deviation away from 8MR centers (toward the guest-rich side) due to the flattened potential well. After the passage of guest molecules, the potential well experienced by the cation is re-established and thus the cation returns to its original energetically favorable site in the center of the 8MR, site SIII′. In contrast, guest molecules such as CH_4 and N_2 that do not facilitate the deviation of door-keeping cations are excluded from entering the supercavity at temperatures below T_S. This selective admission of molecules by the guest-induced temporary and reversible cation deviation process is fundamentally distinct from the conventional molecular sieving achieved by specifically selecting an aperture size between the sizes of the two component gas molecules.[15]

Ab initio DFT calculations were conducted to see if our hypothesis of guest-induced temporary and reversible cation deviation is plausible. Taking CO_2 on **r2**CsCHA as an illustrative example, Figure 4a summarizes the proposed process. First, the presence of the guest molecules such as CO_2 can substantially reduce the energy barrier (ΔE) for the door-keeping cation (Cs^+ in this case) to partially deviate toward the supercavity of the guest-rich side, leaving the 8MR doorway temporarily unobstructed. Then, one of the interacting guest molecules from the guest-rich side moves

toward the 8MR and dwells momentarily at site SIII′. Finally, with the guest molecule moving through the doorway further into the supercavity of the guest-lean side, the cation returns to site SIII′ simultaneously and closes the doorway. We refer to this process as a molecular trapdoor mechanism, taking the analogy to the one used in daily life.

Clearly guest molecules play a key role in changing the energy barrier (and the potential well) for the deviation of door-keeping cations and enable the whole process. Guest molecules with larger electronic quadrupole moment, dipole moment, and polarizability can interact more strongly with the door-keeping cations. Indeed, our DFT calculations show that the energy barriers for cations under the influence of various gases are in the order $\Delta E(CO_2) \ll \Delta E(N_2) \approx \Delta E(CH_4) \approx \Delta E$(vacuum) (Figure 4b). This is consistent with a lower critical admission temperature for CO_2 in our experiments; for example, on **r2**CsCHA, no critical temperature for CO_2 admission was observed down to 200 K (Figure 2b). N_2 and CH_4 have no effect on ΔE (in comparison with vacuum), and thus, their admission occurs only when the spontaneous thermal migration of Cs^+ occurs as explained previously.

We have also examined the mobility of cations in **r2**CsCHA as a function of adsorbed gas by ^{133}Cs nuclear magnetic resonance (NMR) (Figure 3e). There are two different types of peaks: the broad base peak (component 1), which is associated with relatively less mobile Cs^+, and the narrow peak (component 2), associated with mobile Cs^+ that can move between sites. The **r2**CsCHA sample in the CO_2 atmosphere shows a larger relative area of component 2 against that of component 1, suggesting a greater proportion of mobile Cs^+ in the presence of CO_2 than in N_2. Furthermore, both peaks of components 1 and 2 in the presence of CO_2 are narrower than those in N_2, implying that all the Cs^+ in CO_2 atm are more mobile than those in N_2, as the narrower peak represents higher mobility of Cs^+. This finding is consistent with our DFT calculations: the flattened potential well of Cs^+ induced by CO_2 leads to greater Cs^+ mobility.

Only cations residing at the center of 8MRs can function as door-keepers to selectively admit guest molecules. Cations of different sizes and valences exhibit different site preferences and interaction abilities with the local environment.[16] It is known that only K^+,[14] Rb^+,[17] and Cs^+ [13] preferentially coordinate in the center of the 8MRs (site SIII′), while other monovalent cations, including Li^+, Na^+,[14,18] and Ag^+,[19] as well as divalent cations, such as Ca^{2+} [20] and Cu^{2+},[21] reside favorably on other sites (site SI in the D6R, site SII above the D6R, and site SIII next to the 4MR, as shown in Figure S1, Supporting Information), away from the 8MRs. Therefore, we did not observe temperature-dependent admission of gas molecules on Ca^{2+}-exchanged chabazite (N_2 surface area 649 m^2/g).[8] Larger cations experiencing stronger interaction with the local environment of the 8MRs can lead to higher energy barriers ΔE (steeper potential wells), reflected by higher T_C. Our DFT calculations show that the energy barrier for Cs^+ (ΔE = 508 meV) is higher than that for K^+ (ΔE = 278 meV), which is supported by the fact that $T_C(N_2)$ and $T_C(CH_4)$ on **r2**CsCHA (333 and 343 K, respectively) are higher than those on **r2**KCHA (266 and 279 K, respectively) (Figure 2a,b).

The cation density also plays an essential role. Notably, one cation per 8MR at SIII′ is the necessary condition to achieve pore blockage. This quota requires Si:Al $\leq$ 3 in chabazite. For Si:Al > 3, a considerable fraction of unoccupied 8MRs exists, allowing gas molecules to readily pass into the supercavities. The existence of this threshold was validated by comparing N_2 adsorption capacities at 77 K on a series of potassium-exchanged chabazite samples with different Si:Al, in which N_2-accessible surface area was not noticeable until Si:Al exceeded 3 (Table S2, Supporting Information). With the pore aperture completely blocked, a higher density of cations should lead to an increased ΔE due to the electrostatic repulsive interactions among the cations in chabazite. This is consistent with the fact that the critical admission temperature increases with increasing number of cations, namely, $T_C(CO_2)$ on **r1**KCHA (approximately 273 K, Figure 2c) is higher than that on **r2**KCHA (not detected down to 195 K, Figure 2a).

Application for Molecular Separation. Gas mixtures can be efficiently separated by these molecular trapdoor chabazites. For two gases A and B with critical admission temperatures $T_C(A) < T_C(B)$, choosing an appropriate working temperature (T_{work}) between these temperatures allows the zeolite trapdoor to admit gas A but exclude B. For CO_2/CH_4 separation, the highest working temperature is around 233 K on **r2**KCHA with a CO_2/CH_4 selectivity of 98 at 100 kPa based on equimolar single component adsorption capacity (Figure S4, Supporting Information). By choosing a larger cation (**r2**CsCHA), T_{work} increases to around 253 K with a selectivity of 32 (Figure 2d). By increasing the cation density, on **r1**KCHA, T_{work} shifts to above 273 K with a CO_2/CH_4 selectivity of 93 (Figure 2e), which is ideal for separation of industrial methane gases, including biogas, coal seam gas, and natural gas. This CO_2/CH_4 selectivity is, to the best of our knowledge, higher than those of the best physisorbents reported to date under similar conditions available in the literature,[6,22−26] e.g., six for Mg-MOF-74 (273 K, 100 kPa)[26] and 75 for RHO (303 K, 100 kPa).[6] Importantly, the selectivity of our molecular trapdoor chabazite is not compromised even at high pressures, e.g., a record high CO_2/CH_4 selectivity of 21 on **r1**KCHA at 1000 kPa and 273 K (Figure 2e) was recorded, which is crucial for the purification of as-mined natural gas. At higher temperature (303 K), a CO_2/CH_4 selectivity of 20 is also obtained at 400 kPa, which is much larger than the best reported selectivity of 10 on RHO under the same condition.[6] Our molecular trapdoor chabazite also provides exceptionally high adsorption selectivity for CO_2/N_2, e.g. 325 at 20 kPa, 80 at 100 kPa, and 26 at 1000 kPa and 273 K (Figure 2d), corresponding to working conditions found typically in postcombustion carbon capture by vacuum and pressure swing adsorption.[27−29]

To evaluate the performance of our molecular trapdoor materials in a real process of gas mixture separation and to confirm that the trapdoor effect is not compromised in gas mixtures, binary adsorption breakthrough experiments were conducted using a CO_2/CH_4 mixture at 293 K and 116 kPa through both a **r1**KCHA and a **r2**CsCHA column (Figure 5a). Instantaneous elution of CH_4 occurred at the start of the experiments, while CO_2 was detected at the outlet after a substantially longer time, as expected. The resultant CO_2/CH_4 selectivities are 79 and 109, respectively, as determined from mass balance calculations, which is consistent with our prediction based on single component isotherms. This consistency allows us to claim that admission of component A (e.g., CO_2) will not lead to "slipping in" of weak component B (e.g., CH_4) if component B cannot "open" the molecular trapdoor by itself. Our understanding is that immediately after molecule A passes through the 8MR, the steep potential well of the door-keeping cation is re-established, leading to its immediate return to the center of the 8MR. This process is

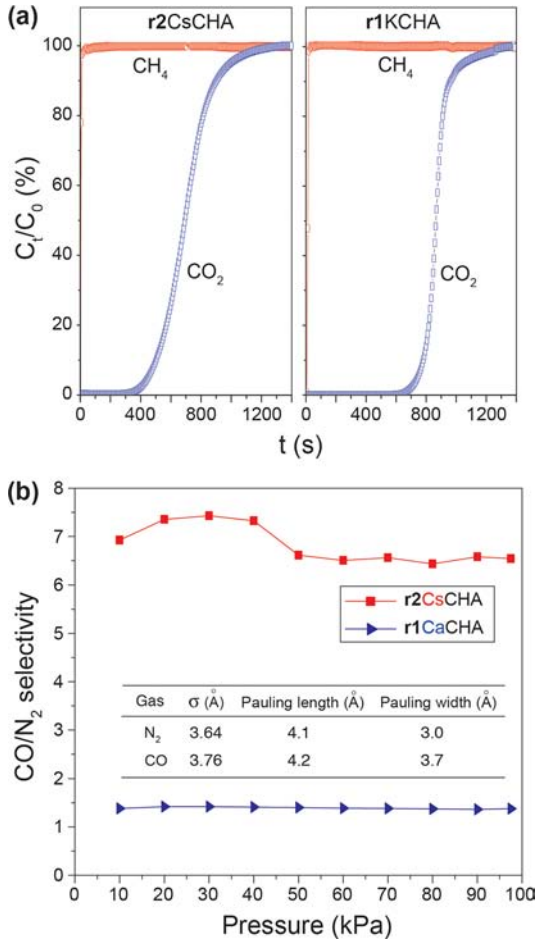

Figure 5. (a) Experimental binary breakthrough curves for a gas mixture of CO_2/CH_4 (15:85 v/v) on our molecular trapdoor chabazites at 293 K and 116 kPa. C_t and C_0 denotes outlet and inlet concentrations, respectively. (b) Selectivities of CO/N_2 on **r2**CsCHA and **r1**CaCHA at 273 K. The adsorption equilibria of chabazites with divalent Ca^{2+} residing at SII (open-pore aperture) show a negligible selectivity between these two gases, indicating no molecular trapdoor effect. Our trapdoor **r2**CsCHA exhibits a counterintuitive size-inverse sieving, selectively admitting CO (larger molecular size) over N_2.

highly energetically favorable compared to passage of molecule B through the 8MR. In addition, our DFT calculations (Figure S5, Supporting Information) show that access to the open 8MR of the weak components (e.g., CH_4 or N_2) is not energetically favorable, in contrast to CO_2, which is in good agreement with a previous report on SSZ-13.[21]

Finally, to further support our contention that separation is not due to molecular size, we show here "size-inverse" separation with our molecular trapdoor materials. An extraordinary example is the exclusive admission of CO (σ = 3.76 Å) over N_2 (σ = 3.64 Å) by **r2**CsCHA (Figures 5b and S6a, Supporting Information). It is known that CO is just marginally stronger in interaction strength with zeolites than N_2 due to their similar properties, reflected by comparable heat of adsorption and low selectivity based on an equilibrium mechanism.[30,31] CO has a slightly higher quadrupole (2.50×10^{-26} esu cm^2 for CO vs 1.52×10^{-26} esu cm^2 for N_2) and polarizability (1.95×10^{-24} cm^3 for CO vs 1.74×10^{-24} cm^3 for N_2) and a moderate dipole (0.11 D for CO). This marginal difference can be dramatically magnified by the molecular trapdoor effect, resulting in remarkably higher selectivity over those zeolites without the trapdoor effect. Admission of CO and exclusion of N_2 was observed on **r2**CsCHA, giving rise to a selectivity of CO/N_2 of about 7 (Figure 5b), whereas both CO and N_2 are adsorbed on open-pore chabazite or other zeolites (where equilibrium mechanism dominates), e.g. **r1**CaCHA (Figure S6b, Supporting Information), giving a selectivity of <1.5 (Figure 5b). Note that this example is just an indication of the potential of the trapdoor effect; much higher selectivity may be achieved by construction of trapdoor zeolite using different frameworks and door-keeping cations. Moreover, separation of CO/H_2 (size-inverse sieving) for syngas purification, CO_2/H_2 (size-inverse sieving) in hydrogen production,[32] and CO_2/O_2 for oxy-fuel recycle combustion may be achieved by using our molecular trapdoor chabazite (Figure S7a–c, Supporting Information), which produces high selectivities of 13, 95, and 90, respectively, at atmospheric pressure. In these cases we hypothesize that H_2 is rejected by the molecular trapdoor mechanism even at room temperature on the basis of our DFT calculation that the energy barrier (ΔE) for H_2 is similar to that for N_2 ($T_C \sim 333$ K); we are currently testing this hypothesis. These examples demonstrate that molecular size is not the controlling factor for separation on our chabazite materials.

We contend that the molecular trapdoor mechanism may be an important underlying mechanism on other zeolites with door-keeping cations, such as RHO and LTA. One of the examples is Cs^+-containing zeolite RHO on which the highly selective separation of CO_2/CH_4 was attributed to molecular sieving.[6] However, the fact of exclusive admission of CO_2 over CH_4 via completely cation-blocked 8MRs suggests the separation may actually be governed by a molecular trapdoor mechanism.

CONCLUSION

We have uncovered a new mechanism for molecular separation by a particular family of zeolites, where gas molecules having sufficient interaction ability to induce the door-keeping cations to deviate from the center of pore apertures (temporarily and reversibly) can be exclusively admitted. These zeolites are better referred to as molecular trapdoor than molecular sieve zeolites, as discrimination is not on the basis of size. This molecular trapdoor mechanism also suggests that use of probe molecules of a particular size to infer pore aperture size should be applied with caution. Our molecular trapdoor chabazite materials exhibit record high selectivity for separation of important industrial gas mixtures such as CO_2/CH_4 and counterintuitive size-inverse sieving of CO/N_2 and are currently under investigation for industrial pressure swing adsorption processes. The molecular trapdoor mechanism paves a new route to design materials for high performance adsorption, membrane, and catalysis processes.

EXPERIMENTAL SECTION

Zeolite Syntheses and Ion Exchange. Chabazite with Si:Al = 2 was synthesized from zeolite Y (CBV400) following the reported procedure with gel composition $0.17Na_2O{:}2.0K_2O{:}Al_2O_3{:}5.18SiO_2{:}224H_2O$.[33] A typical procedure involved addition of 25 g of zeolite Y powder to 198.2 mL of deionized water and 9.5 M KOH (26.8 mL) in a polypropylene bottle. The mixture was shaken for about 30 s and placed in an oven for 15 d at 368 K. The product obtained was filtered, washed with deionized water, and dried in an oven at 373 K.

Chabazite with Si:Al = 1 was synthesized by enriching Al content of chabazite with Si:Al = 2 following the reported procedure[34] with some modification. A typical procedure involved slurrying 30 g of as-synthesized chabazite with Si:Al = 2, 13.2 g of NaOH, and 16.8 g of

dx.doi.org/10.1021/ja309274y | J. Am. Chem. Soc. 2012, 134, 19246–19253

alumina hydroxide (50−57 wt % Al_2O_3) in 120 mL of deionized water for 72 h at 346 K in a Parr autoclave under stirring (45 rpm). The resultant product was filtered, washed with deionized water, and dried in an oven at 373 K. The Si:Al ratio was confirmed by ^{27}Al and ^{29}Si NMR (Figure S8, Supporting Information).

Chabazite with Si:Al = 1.5 was synthesized using a procedure similar to that for chabazite with Si:Al = 1; the Al amount was adjusted as required.

Chabazite with Si:Al = 5.4, 17, and 50 were synthesized following the reported procedure.[35] Chabazites with Si:Al = 6.5 and 7 were synthesized following a different reported procedure.[36]

The as-synthesized chabazite was ion-exchanged to the respective cation forms (K^+, Cs^+, or Ca^{2+}) as follows: 200 mL of 1 M KCl, CsCl, or $CaCl_2$ was added to 5 g of as-synthesized chabazite (solution-to-zeolite ratio of 40) and the mixture was refluxed at 343 K under stirring for 24 h. The supernatant solution was decanted and the solid was washed three times with deionized water. The above procedure was repeated five times. The products were dried in an oven at 353 K.

Sample Activation. Zeolite samples were heated stepwise, thoroughly dehydrated, and degassed at 623 K under vacuum for 18 h before measurements.

Gas Adsorption Experiments. Adsorption isotherms for gases on activated zeolites were measured over 77−423 K and at pressures up to 120 kPa on a Micromeritics ASAP2010. High-pressure adsorption isotherm measurements (1000 kPa) were performed on a Micromeritics ASAP2050.

Nuclear Magnetic Resonance. Unactivated **r2**CsCHA was packed into NMR rotors and spun. The caps were removed, and the samples in the rotors were activated following the standard activation procedure (as above), cooled to room temperature, and backfilled with the appropriate gas at 393 K. Rotor caps were then quickly fitted, operating under a stream of the appropriate gas in a glovebag.

Static ^{133}Cs NMR experiments were carried out at 9.1 T on a Bruker Avance 400 spectrometer operating at 52.5 MHz and referenced to dilute CsCl (aq) at 0 ppm. **r2**$CsCHA/N_2$ and **r2**$CsCHA/CO_2$ were measured using an Oldfield Echo pulse sequence (two $\pi/6$ pulses separated by 200 μs, followed by acquisition of the echo signal), with a 10 s recycle delay.

^{29}Si and ^{27}Al spectra of **r2**$CsCHA/H_2O$ were measured at 7.1 T on a Bruker Avance spectrometer with a 4 mm MAS probe at spinning speeds of 10−14 kHz, using a single pulse sequence. Recycle delays and references were 5 s and tetramethylsilane (^{29}Si) and 20 s and aqueous $Al(NO_3)_3$ (^{27}Al).

Positron Annihilation Lifetime Spectroscopy. Positron annihilation lifetime spectroscopy (PALS) is used to investigate free volume within materials (pores <20 nm). The lifetime of positrons within the sample is used to calculate average pore sizes, while the intensity provides information on the relative number of pores. Spectra were measured on an EG&G Ortec fast−fast coincidence system using $^{22}NaCl$ as the positron source. Samples were packed around the source in a N_2 glovebox and analyzed under vacuum (5×10^{-7} Torr) with increasing temperature. A minimum of five spectra were collected with 4.5×10^6 counts in each spectrum. Spectra were fitted to four components using LT9 software, indicating the presence of two different pore sizes within the zeolite samples; τ_3 was associated with the pores within the zeolite cages and τ_4 was related to larger intercrystalline micropores.

In situ Synchrotron X-ray Diffraction of Gas Adsorption. High-resolution in situ synchrotron X-ray powder diffraction data were collected on the Powder Diffraction Beamline, Australian Synchrotron, using a Mythen-II detector. For XRD phase identification, chabazite samples were ground with a pestle and mortar and then loaded under argon into 0.7 mm special glass capillaries and sealed with wax. For in situ measurements, the sample containing capillary was mounted into an in-house designed flow cell with connection to different gas lines and vacuum via selective valves/needle valves. The sample cell was temperature controlled from 195 to 500 K using an Oxford Cryostream. The sample was in situ activated by heating stepwise (10 K/min) to 623 K and held at 623 K for 4 h before analysis. Then the sample was measured under vacuum with decreasing temperature and then under N_2 flow (1 bar) and then CO_2 (1 bar). Between the two atmospheres, the sample was reactivated as above. The cooling/heating rate was 6 K min^{-1}, and data were collected for 10 min at each point. The wavelength for all these measurements was 0.8268 Å.

Binary Breakthrough. Gas separation properties of chabazites were examined by binary breakthrough experiments using CO_2/CH_4 (15:85 v/v) gas mixtures. Argon was used as an internal standard. **r1**KCHA (4.96 g) and **r2**CsCHA (4.13 g) were preactivated at 623 K under vacuum on a Micromeritics ASAP2050 for 24 h and then transferred into a stainless-steel column (3/8 in. diameter, 16 cm long) and activated in situ at 573 K under vacuum overnight. It must be noted that, at the end of activation step, backfill with inert gas to the sample was conducted only after the sample was fully cooled to room temperature. Separations were carried out at 293 K with dosing the gas mixture (116 kPa) at a flow rate of 40 mL/min at STP controlled by mass flow controllers. Relative amounts of gases passing through the column were measured by a mass spectrometer (Pfeiffer Vacuum) detecting ion peaks at m/z = 44, 28, and 12 for CO_2 and m/z = 14 and 13 for CH_4.

■ DENSITY FUNCTIONAL THEORY CALCULATIONS

Ab initio density functional theory (DFT) calculations were employed to determine the chabazite structure, cation location, and occupancy, as well as gas adsorption configuration. We used the Vienna Ab initio Simulation Package (VASP)[37] with the generalized gradient approximation (GGA)[38] and the projector augmented waves (PAW) approach.[39] The cutoff energy of the plane wave basis-set was 600 eV. A γ-point-only k-point mesh was used for one unit cell of chabazite (including three double-six ring prisms). Such cutoff energy and k-point mesh have been tested to ensure the total energy convergence within 1 meV/atom. The atomic positions were optimized with the conjugate gradient method until the forces acting on atoms were below 0.015 eV/Å, as suggested by Göltl and Hafner.[40]

We applied the nudged-elastic-band (NEB) method for energy barrier calculations. Figure S3 (Supporting Information) shows the energy profile for migration of a single Cs cation in chabazite unit cell from SIII′ to SII. We observed a very shallow potential well at site SII. Thus for simplicity, the difference in the total energy in the case of Cs^+ at site SIII′ and that of Cs^+ at site SII was used to approximate the migration energy barrier of the Cs cation (summarized in Table S1 (Supporting Information) and demonstrated in Figure 4).

■ ASSOCIATED CONTENT

Ⓢ Supporting Information

More adsorption isotherms, ^{27}Al and ^{29}Si NMR, synchrotron PXRD and DFT calculations. This material is available free of charge via the Internet at http://pubs.acs.org.

■ AUTHOR INFORMATION

Corresponding Author

paul.webley@unimelb.edu.au; zhe.liu@monash.edu

Author Contributions

◆These authors contributed equally.

Notes

The authors declare no competing financial interest.

■ ACKNOWLEDGMENTS

Funding for this CO2CRC project is provided by the Australian Government through its CRC program. We acknowledge Monash University and the NCI National Facility at the ANU. This research was undertaken on the powder X-ray diffraction

beamline at the Australian Synchrotron, Victoria, Australia. We thank Y. Yang, J. Patel, S. Wang, and N. Burke from CSIRO for help with breakthrough experiments. We are grateful to Z. Wu and P. Xiao for comments. We thank D. Kearley from ANSTO for discussions. T.J.B., C.M.D., and A.J.H. acknowledge the CSIRO OCE Science Leader Scheme for support.

REFERENCES

(1) Breck, D. W. *Zeolite Molecular Sieves: Structure, Chemistry, and Use*; Wiley: New York, 1974.
(2) Kuznicki, S. M.; Bell, V. A.; Nair, S.; Hillhouse, H. W.; Jacubinas, R. M.; Braunbarth, C. M.; Toby, B. H.; Tsapatsis, M. *Nature* **2001**, *412*, 720−724.
(3) Yuan, W.; Lin, Y. S.; Yang, W. *J. Am. Chem. Soc.* **2004**, *126*, 4776−4777.
(4) Yakubovich, O. V.; Massa, W.; Gavrilenko, P. G.; Pekov, I. V. *Crystallogr. Rep.* **2005**, *50*, 544−553.
(5) Firor, R. L.; Seff, K. *J. Am. Chem. Soc.* **1977**, *99*, 6249−6253.
(6) Palomino, M.; Corma, A.; Jordá, J. L.; Rey, F.; Valencia, S. *Chem. Commun.* **2012**, *48*, 215−217.
(7) Lobo, R. F. *Handbook of Zeolite Science and Technology*; Auerbach, S. M., Carrado, K. A., Dutta, P. K., Eds.; CRC Press: New York, 2003; pp 65−90.
(8) Shang, J.; Li, G.; Singh, R.; Xiao, P.; Liu, J. Z.; Webley, P. A. *J. Phys. Chem. C.* **2010**, *114*, 22025−22031.
(9) The selectivity of component A against component B is defined as $(x_A/y_A)/(x_B/y_B)$, where x denotes adsorbed-phase concentration and y denotes the corresponding gas-phase concentation.
(10) Breck, D. W.; Smith, J. V. *Sci. Am.* **1959**, *200*, 85−94.
(11) Woodcock, D. A.; Lightfoot, P.; Villaescusa, L. A.; Díaz-Cabañas, M.-J.; Camblor, M. A.; Engberg, D. *Chem. Mater.* **1999**, *11*, 2508−2514.
(12) At ordinary temperature, molecules up to 0.5 Å wider than the diameter of the aperture can pass through, caused by the pulsation of the aperture and kinetic energy of the incoming molecules (ref 10).
(13) Calligaris, M.; Mezzetti, A.; Nardin, G.; Randaccio, L. *Zeolites* **1986**, *6*, 137−141.
(14) Smith, L. J.; Eckert, H.; Cheetham, A. K. *Chem. Mater.* **2001**, *13*, 385−391.
(15) Maes, M.; Alaerts, L.; Vermoortele, F.; Ameloot, R.; Couck, S.; Finsy, V.; Denayer, J. F. M.; De Vos, D. E. *J. Am. Chem. Soc.* **2010**, *132*, 2284−2292.
(16) Yang, R. T. *Adsorbents: Fundamentals and Applications*; John Wiley & Sons, Inc.: Hoboken, NJ, 2003.
(17) Saxton, C. G.; Kruth, A.; Castro, M.; Wright, P. A.; Howe, R. F. *Microporous Mesoporous Mater.* **2010**, *129*, 68−73.
(18) Smith, L. J.; Eckert, H.; Cheetham, A. K. *J. Am. Chem. Soc.* **2000**, *122*, 1700−1708.
(19) Calligaris, M.; Mezzetti, A.; Nardin, G.; Randaccio, L. *Zeolites* **1984**, *4*, 323−328.
(20) Mortier, W. J.; Pluth, J. J.; Smith, J. V. *Mater. Res. Bull.* **1977**, *12*, 97−102.
(21) Hudson, M. R.; Queen, W. L.; Mason, J. A.; Fickel, D. W.; Lobo, R. F.; Brown, C. M. *J. Am. Chem. Soc.* **2012**, *134*, 1970−1973.
(22) Anson, A.; Lin, C. C. H.; Kuznicki, S. M.; Sawada, J. A. *Chem. Eng. Sci.* **2009**, *64*, 3683−3687.
(23) Zhang, J.; Wu, H.; Emge, T. J.; Li, J. *Chem. Commun.* **2010**, *46*, 9152−9154.
(24) Cavenati, S.; Grande, C. A.; Lopes, F. V. S.; Rodrigues, A. E. *Microporous Mesoporous Mat.* **2009**, *121*, 114−120.
(25) Couck, S.; Denayer, J. F. M.; Baron, G. V.; Rémy, T.; Gascon, J.; Kapteijn, F. *J. Am. Chem. Soc.* **2009**, *131*, 6326−6327.
(26) Britt, D.; Furukawa, H.; Wang, B.; Glover, T. G.; Yaghi, O. M. *Proc. Natl. Acad. Sci. U. S. A.* **2009**, *106*, 20637−20640.
(27) Zhang, J.; Webley, P. A.; Xiao, P. *Energy Conv. Manage.* **2008**, *49*, 346−356.
(28) Ruthven, D. M.; Farooq, S.; Knaebel, K. S. *Pressure Swing Adsorption*; VCH Publishers: New York, 1994.
(29) Zhang, J.; Webley, P. A. *Environ. Sci. Technol.* **2007**, *42*, 563−569.
(30) Sethia, G.; Dangi, G. P.; Jetwani, A. L.; Somani, R. S.; Bajaj, H. C.; Jasra, R. V. *Sep. Sci. Technol.* **2010**, *45*, 413−420.
(31) Lopes, F. V. S.; Grande, C. A.; Ribeiro, A. M.; Loureiro, J. M.; Evaggelos, O.; Nikolakis, V.; Rodrigues, A. E. *Sep. Sci. Technol.* **2009**, *44*, 1045−1073.
(32) Herm, Z. R.; Swisher, J. A.; Smit, B.; Krishna, R.; Long, J. R. *J. Am. Chem. Soc.* **2011**, *133*, 5664−5667.
(33) Bourgogne, M.; Guth, J. L.; Wey, R. Process for the preparation of synthetic zeolites, and zeolites obtained by said process. U.S. Patent 4,503,024, 1985.
(34) Thrush, K. A.; Kuznicki, S. M. *J. Chem. Soc. Faraday Trans.* **1991**, *87*, 1031−1035.
(35) Zones, S. I. Zeolite SSZ-13 and its method of preparation. U.S. Patent 4,544,538, 1985.
(36) Zones, S. I. *J. Chem. Soc. Faraday Trans.* **1991**, *87*, 3709−3716.
(37) Kresse, G.; Furthmüller, J. *Phys. Rev. B* **1996**, *54*, 11169−11186.
(38) Perdew, J. P.; Burke, K.; Ernzerhof, M. *Phys. Rev. Lett.* **1996**, *77*, 3865−3868.
(39) Kresse, G.; Joubert, D. *Phys. Rev. B* **1999**, *59*, 1758−1775.
(40) Göltl, F.; Hafner, J. *J. Chem. Phys.* **2011**, *134*, 0641021−06410211.